Int J Earth Sci (Geol Rundsch) (2014) 103:1023–1036
DOI 10.1007/s00531-014-1020-y

ORIGINAL PAPER

Origin and age of ultramafic rocks and gabbros in the southern Puna of Argentina: an alleged Ordovician suture revisited

Udo Zimmermann · Heinrich Bahlburg · Klaus Mezger · Jasper Berndt · Suzanne Mahlburg Kay

Received: 27 November 2013 / Accepted: 23 March 2014 / Published online: 10 April 2014

Abstract Ultramafic rocks and gabbros are exposed in the southern Puna (NW Argentina) in tectonic association with continental arc-related Ordovician (volcano) sedimentary successions and granitoids. The origin of this mafic rock suite has been debated for three decades as either representing an Ordovician terrane suture, primitive Ordovician arc-related rocks or relics of the pre-Ordovician basement in tectonic contact with the Ordovician retro-arc basin successions. We present the first U–Pb ages of primary and inherited zircon from gabbros of this mafic–ultramafic assemblage. LA-ICP-MS analyses on cores and rims of these zircon grains yielded a concordia age of 543.4 ± 7.2 Ma for the gabbroic rocks. Other analysed zircons have Mesoproterozoic, and Early Ediacaran core and rim ages indicating that the magmas also assimilated Meso- and Neoproterozoic crustal material prior to final crystallization. The mafic rocks witnessed higher metamorphic grade than associated Ordovician rocks, which are unmetamorphosed or only affected by anchimetamorphism. The gabbros are mostly tholeiitic and enriched in Zr, Th, as well as other incompatible elements and have $\varepsilon Nd_{t=540Ma}$ ranging from 1.3 to 7.4 with most of the values between 5 and 7. $^{147}Sm/^{144}Nd$ ratios show evidence of weak crustal contamination. The mafic rocks do not reveal any affinity to mid-ocean ridge basalts in their geochemistry but point instead to an emplacement in an active plate margin arc environment. Chromites from ultramafic rocks show typical Ti, Al, Cr#, Fe^{3+} abundances found in magmatic arc rocks. The formation of the gabbros and the associated ultramafic rocks in the southern Argentine Puna is related to the evolution of the margin of the Pampia terrane, including the Puncoviscana basin, during the Late Neoproterozoic and earliest Cambrian. In contrast to previous interpretations, the rocks predate the Ordovician evolution of the Central proto-Andean active margin. Consequently, interpretations assuming these rocks to represent an oceanic terrane suture of Ordovician age have to be dismissed as much as all palaeotectonic models that define Ordovician terranes in the Central Andes based on assumption that the ultramafic rocks and gabbros exposed in the southern Puna mark plate boundaries.

Keywords Argentina · Western Gondwana margin · Puna–Famatina magmatic arc · Ultramafic and mafic rocks · Pampia Terrane

Electronic supplementary material The online version of this article (doi:10.1007/s00531-014-1020-y) contains supplementary material, which is available to authorized users.

U. Zimmermann (✉)
Department of Petroleum Engineering National IOR Center, University of Stavanger, 4036 Stavanger, Norway
e-mail: udo.zimmermann@uis.no

H. Bahlburg
Institut für Geologie und Paläontologie, Westfälische Wilhelms-Universität, Corrensstrasse 24, 48149 Münster, Germany

K. Mezger
Institute of Geological Sciences, University of Bern, Baltzerstrasse 1+3, 3012 Bern, Switzerland

J. Berndt
Institut für Mineralogie, Westfälische Wilhelms-Universität, Corrensstrasse 24, 48149 Münster, Germany

S. M. Kay
Department of Geological Sciences, Cornell University, Ithaca, NY 14853, USA

Introduction

In ancient mountain belts, collision zones between different plates or tectonostratigraphic terranes are commonly marked by ophiolites (Howell et al. 1985). These sutures contain dismembered ophiolite assemblages made up of peridotites, gabbros and sheeted dike complexes overlain by pillow basalts associated with marine, commonly pelagic, sedimentary rocks (e.g. Robertson and Xenophontos 1997; Dilek and Newcomb 2003; Wright and Shervais 2008). Complete ophiolite sequences are preserved in some locations, although commonly tectonic dismemberment, related to the emplacement of the ophiolite, leads to the preservation of variable partial combinations of ophiolite lithologies. A further feature of dismembered ophiolites is the presence of thrusts and relatively broad zones of tectonic mélanges in which sheared ophiolite lithologies are mixed with deposits of deep marine or marginal sedimentary facies (Aalto 1982; Howell et al. 1985; Keppie 1989).

In the southern Puna of northwest Argentina (Fig. 1), assemblages of mafic and ultramafic rocks occur in several localities in tectonic association with Ordovician marine silici- and volcaniclastic units (Argañaraz et al. 1973; Coira 1974; Allmendinger et al. 1982; Zappettini et al. 1994; Coira et al. 1999; Zimmermann and Bahlburg 2003). On the basis of field observations alone, these rocks were interpreted as ophiolites marking either the Ordovician active margin of Gondwana in this region (since Allmendinger et al. 1982) or

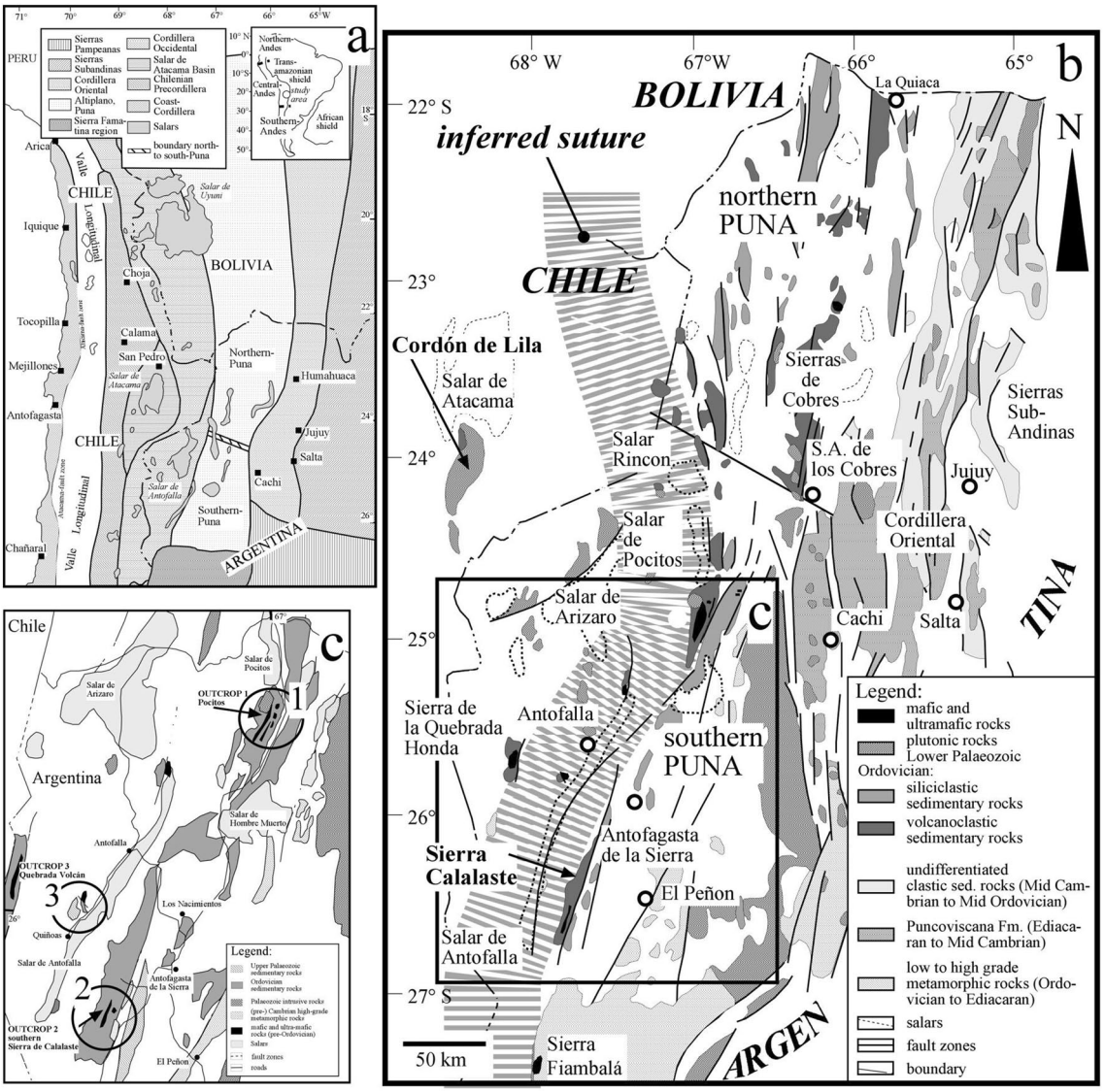

Fig. 1 **a** Geotectonic units in the Central Andes (after Bahlburg and Hervé 1997). **b** Geological map of the Puna (revised after Rapela et al. 1992; Coira et al. 1999). **c** Outcrop location in the southern Puna are encircled: *1* Pocitos, *2* Southern Sierra de Calalaste, *3* Quebrada Volcán. Detailed maps of the exposures can be found in Fig. 1 data repository

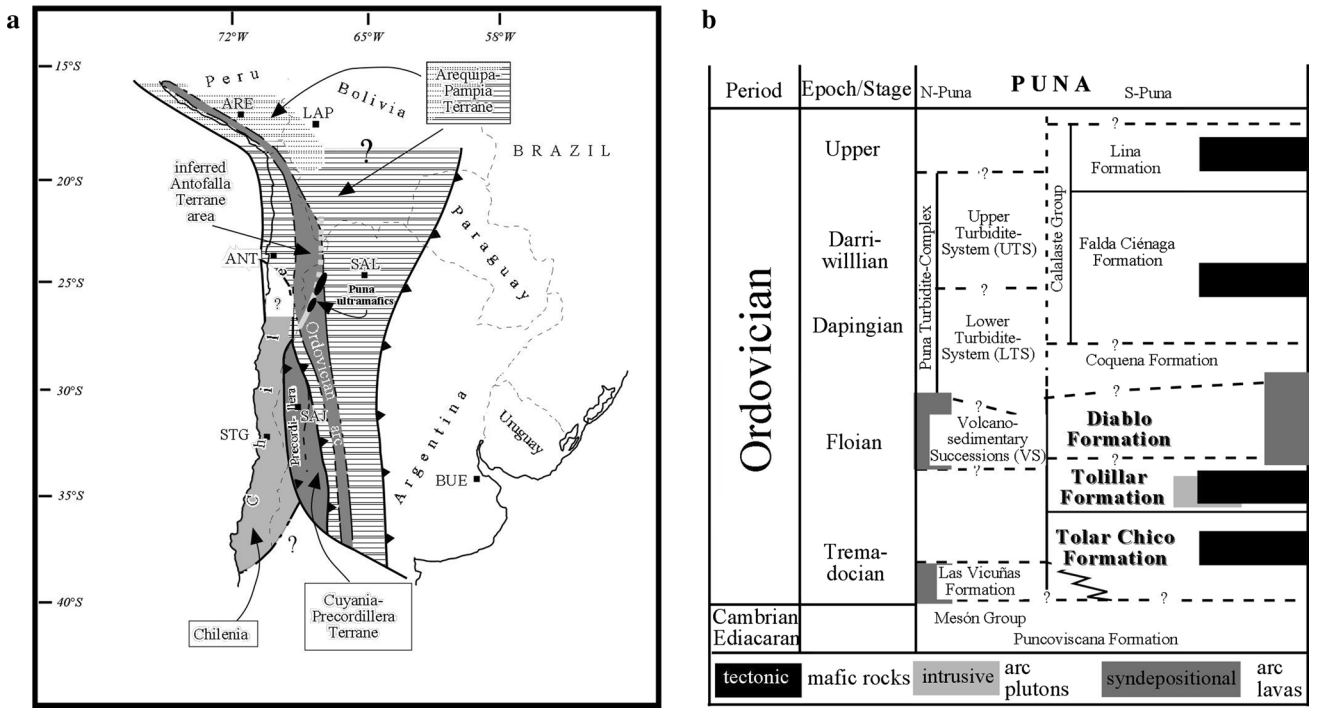

Fig. 2 **a** Terrane map of NW Argentina (from Bahlburg et al. 2009). (*ANT* Antofagasta de Chile, *ARE* Arequipa, *BUE* Buenos Aires, *LAP* La Paz, *SAJ* San Juan, *SAL* Salta, *STG* Santiago de Chile. **b** Detailed stratigraphic relations of magmatic and sedimentary rocks in the Puna region and the regional tectono-magmatic framework (revised after Bahlburg and Hervé 1997; Zimmermann and Bahlburg 2003). Note that the here shown mafic rocks are not of Ordovician age but in tectonic contact with the shown formations

the Late Ordovician suture zone along which the allochthonous Arequipa terrane or Arequipa–Antofalla block collided with the proto-Andean active margin (Martos 1982; Dalziel and Forsythe 1985; Palma et al. 1990; Rapela et al. 1992; Forsythe et al. 1993; Blasco et al. 1996; Conti et al. 1996; Ramos 1988, 1996, 2008; Rapalini 2005; Ramos et al. 2010; Fig. 2a). Recent models propose that the rocks in question are related to the Ordovician continental arc system (Coira et al. 2009a, b). In view of the poorly constrained age of the alleged ophiolite assemblages, Mon and Hongn (1991) argued on the basis of structural data for a pre-Ordovician age for most of the mafic succession. These authors concluded that the rocks' formation was older than and independent from the Ordovician tectonic setting. This interpretation was supported by Zimmermann and Bahlburg (2003) based on provenance data of the host rocks. All mentioned models of terrane accretion during the Lower Palaeozoic in this region and along the alleged suture largely ignore the sedimentological architecture of the Ordovician successions and the evolution of the respective basin in northwest Argentina and northern Chile (Bahlburg 1990, 1998; Bock et al. 2000; Zimmermann and Bahlburg 2003; Zimmermann et al. 2010). The Ordovician geological record of the region can be understood in terms of a single active continental margin basin occupying the southwestern Gondwana margin in the southern Central Andes of northern Chile and northwest Argentina (Bahlburg 1990, 1998; Bahlburg and Hervé 1997; Bock et al. 2000; Lucassen et al. 2000; Egenhoff and Lucassen 2003; Zimmermann and Bahlburg 2003, 2005; Egenhoff 2007; Zimmermann et al. 2010; Fig. 1a, b).

This contribution presents the first U–Pb age data from zircon grains from gabbros of the mafic–ultramafic assemblage in the southern Puna of Argentina. We combine the age constraints with geochemical data on this assemblage in order to analyse their origin and the tectonic setting of their emplacement. These data are used to discriminate between and test the proposed models of the origin of the studied rocks.

Geological setting of the mafic successions in the southern Puna

Assemblages of ultramafic, mafic, intermediate and sedimentary rocks occur in the southern Puna of Argentina in four outcrop regions (Fig. 1). The complex structural Phanerozoic geological history of this region comprises three larger tectonic events during the Ordovician, Upper Palaeozoic and Cenozoic (Ramos 1999), which could have modified or destroyed any indicator for possible primary intrusive or tectonic contacts. Detailed studies on the sedimentary rocks at the contacts with the mafic rocks did not

reveal any contact metamorphic phenomena, but mylonites and talc-rich contact zones of 0.5-m thickness are commonly exposed (Zimmermann 1999). In the southern Sierra de Calalaste, contact metamorphism of sedimentary rocks of presumed Ordovician age (Zimmermann 1999; Zimmermann and Van Staden 2002b) caused by mafic rocks was observed by Quenardelle and Poma (2008). However, Cretaceous mafic rocks are reported in the Central Andes (Lucassen et al. 2007) and can be easily confused with those of older successions. We mapped three of the assemblages in detail, the 'Complejo Ojo de Colorados' (Zappettini et al. 1994) to the south of the Salar de Pocitos, the 'Complejo Básico-Ultrabásico Tramontana' in the southern Sierra de Calalaste (Seggiaro et al. 2002; Fig. 1c) and the mafic rocks of the Quebrada Volcán (Zimmermann 1999; Zimmermann and Van Staden 2002a, b). The fourth outcrop with presumably similar assemblages in the Sierra de la Quebrada Honda (Fig. 1b) is very remote and has been visited and studied only briefly.

The mafic rocks underwent a higher grade of metamorphism than the very low-grade metamorphic sedimentary host rocks (Zimmermann 1999; Zimmermann and Bahlburg 2003; Quenardelle and Poma 2008) and show strong hydrothermal overprinting. In one exposure continental arc-related granitoids of the 'Complejo Ígneo Pocitos' (Zappettini et al. 1994; Kleine et al. 2004; Fig. 1a data repository), have intruded the mafic rocks ('Complejo Ojo de Colorados') and the sedimentary rocks of the Tolillar Formation at 476 ± 2 (U–Pb on titanites; Kleine et al. 2004). The latter is dated into the Lancefield 2 (Late Tremadoc) by the occurrence of *Araneograptus murrayi* (Hall, 1865; Lindholm, 1991; Zimmermann et al. 1998; Fig. 2b).

Exposures and petrography of the mafic rocks

Salar de Pocitos

The 'Complejo Ojo de Colorados' of Zappettini et al. (1994; Fig. 1c, a data repository) represents a dismembered body and consists of gabbros, monzogabbros, ultramafic cumulate rocks and serpentinites penetrated by different dike generations of different ages based on field relations. Outcrops range from 10 × 200 m to 2,000 × 500 m for the gabbros and monzonites and form hills abruptly rising c. 300 m above the local base level of c. 4,000 m. Cumulate rocks and serpentinites occur only in very small lenses of 10 × 5 m as bodies in the gabbros and are never in contact with the sedimentary rocks. The contacts between the gabbros and the ultramafic (cumulate) bodies are not exposed. The mafic rocks are interlayered tectonically with the sedimentary host rocks of latest Tremadoc age, either the Tolar Chico Formation or the Tolillar Formation (Zimmermann et al. 1998; Fig. 2b; Fig. 1a data repository.)

The monzogabbros are coarse-grained, rich in plagioclase and alkali feldspar. The latter can be up to 2 cm in diameter, plagioclase is smaller. The plagioclase is weathered, saussuritised and variably altered to sericite or calcite and associated with amphiboles. Orthopyroxene and zircon are accessory phases. The zircon crystals are small and mostly rounded. Secondary minerals are epidote, chlorite, amphibole and pumpellyite. The gabbros are fine to medium grained and consist mainly of hypidiomorphic plagioclase, which may be altered and saussuritised, small hornblende crystals partly with feldspar overgrowths, pyroxene (partly replaced by tremolite) and olivine. Accessory phases are orthopyroxene and small, slightly rounded but broken zircon grains. The groundmass comprises small plagioclase laths and amphibole. As secondary phases occur serpentine, chlorite-epidote-phyllosilicate intergrowths, magnetite and opaque phases. The ultramafic rocks have a harzburgitic to lherzolitic composition and represent basal cumulates. Olivine (70–85 % of the whole rock) is partially transformed to serpentine. Besides olivine, orthopyroxene and magnetite are common. Small olivine crystals contain chromite inclusions. Accessory minerals include clinopyroxene and small plagioclase grains. Pyroxene shows alteration to tremolite. Secondary minerals are large brown amphibole, chlorite and serpentine.

Sierra de Calalaste

In the southern Sierra de Calalaste, monzogabbros, gabbros and ultramafic cumulate rocks of the 'Complejo Básico-Ultrabásico Tramontana' (Seggiaro and Becchio 1999; Fig. 1c, b data repository) occur in sheared, lenticular, layered intrusive bodies covering an area of 6 km × 300 m, and in isolated smaller outcrops (Fig. 1b data repository). Ultramafic rocks usually form small lenses within the mafic and intermediate intrusive bodies with tectonised contacts, which makes any interpretation of the nature of the contacts impossible. The biggest ultramafic rock body covers an area not larger than 150 × 300 m. Thick (~30 m) mylonitic bands occur in greywackes, which are in other areas mottled rocks, were recognised (Zimmermann 1999) and then recently interpreted as resulting from an intrusive emplacement of mafic rocks of unknown age and geochemical characteristics (Quenardelle and Poma 2008), and might be related to Mesozoic mafic intrusive activity like the Pocitos region. Other contacts show a development of talc-rich zones between gabbros and sandstones as a result of the emplacement mechanism and subsequent multiple deformation, masking the original emplacement process.

Monzogabbros are medium to coarse grained and characterised by large plagioclase crystals. Alkali feldspars are smaller and less abundant, as are hornblende and pyroxene. Plagioclase is partly altered and saussuritised. Pyroxene is commonly replaced by tremolite. Orthopyroxene is less abundant and smaller than clinopyroxene. Accessory phases are small plagioclase laths and minute zircon. Secondary minerals are chlorite, epidote, magnetite and possible haematite. Gabbros are fine to medium grained, composed of plagioclase laths and are, compared to the monzogabbros, richer in hornblende and clinopyroxene. Plagioclase is partly altered and saussuritised, replacement by clinozoisite, chlorite and calcite is common. Pyroxene is commonly replaced by tremolite. Accessory minerals are olivine and alkali feldspar. Olivine is small and mostly altered to serpentine or chlorite. As secondary minerals, chlorite and amphibole have been identified. The ultramafic rocks are lherzolites or olivine-websterites and have a porphyric texture with phenocrysts of clinopyroxene (augite and diopside), orthopyroxene (hypersthene) and olivine (forsterite). Hypersthene commonly contains small inclusions of serpentinised olivine. Serpentinisation of olivine is common; olivine and pyroxene also may be partly replaced by chlorite and the biotite-phlogopite series. Skeletal magnetite is a common mineral. In some samples, pyroxene is partly replaced by tremolite. Accessory plagioclase is altered to sericite and calcite. Secondary minerals are serpentine and chlorite.

Quebrada Volcán

The rocks are exposed in two areas. One larger outcrop (800 × 200 m minimum) is in tectonic contact with pre-Ordovician red pelites (Zimmermann and Van Staden 2002a; Zimmermann 2005) and composed of very fine- to coarse-grained mafic rocks (VO and VGS in Table 1 supplementary material and all figures). The second exposure (2,000 m × 500 m minimum) is further towards the west and separated from the other gabbros and pre-Ordovician successions by Cenozoic volcanic rocks. These rocks are strongly tectonised and only coarse-grained gabbro occurs (EV in Table 1 supplementary material and all figures).

Some of the mafic rocks are fine-grained and strongly affected by chloritisation, which destroyed any primary textures and hampers mineral identification. The rocks display a fine mesh of green-black and white minerals in the polarisation microscope and minute quartz. Strongly altered (saussuritised and sericitised) plagioclase is abundant. Pyroxene (commonly altered to hornblende, which in turn is again strongly altered), olivine and alkali feldspar are rare. Magnetite and quartz occur as secondary phase besides abundant chlorite.

Analytical methods

X-ray diffraction

Samples have been pulverised in an agate beaker with an agate pestle to very fine grain sizes. Then, they have been placed in random mounts were analysed on a Siemens D 5000 (University of Heidelberg, Germany), with Cu Kα X-ray radiation, Ni filter, Si monochromator, at 40 kV and 30 mA. Step scan at ~1.5°/min with a step size of 0.02° 2θ.

Major and trace element analyses

Samples were cleaned before geochemical analyses, and the weathering surfaces were removed. Only homogeneous samples were selected, crushed and milled in an agate mill to a very fine powder (<2 μm). Fusion disks were prepared with Spektroflux 100 (lithiumtetraborate) as flux. *X-Ray fluorescence (XRF)* analyses (University of Heidelberg, Germany) for major and trace elements were carried out using a SRS 303 (Siemens) wavelength-dispersive XRF spectrometer operating at 50 kV and 50 mA. Detection limits are related to the atomic number, and between 1 and 10 μg/g for heavy elements. Precision is between 0.5 and 2 % (1σ), accuracy was controlled by repeated measurements of standards and each sample was measured two times. Some trace element and major element analyses were carried out by ICP-MS at ACME Laboratories (Vancouver, Canada). Detection limits and preparation procedures can be downloaded from www.acmelab.com. INAA analyses were performed by ACTLABS (Ontario, Canada) and for some samples at Cornell University according to standard methods. Detection limits are between 0.5 and 5 ppm for elements like Ag and Cr. INAA precision based on replicate analyses of international rock standards is 2–5 % (1σ). Further information about detection limits and methodology can be downloaded from www.actlabs.com. Trace elements measured at Cornell University were done by INAA at Ward Laboratory at Cornell University. Further information on INAA analyses at Cornell University, and the use of Fe as an internal flux monitor can be found in Kay et al. (1987).

Electron microprobe analysis

Quantitative analyses of chromite were carried out on a Cameca Cambax 355 electron microprobe with Oxford link integrated WDS, set at a voltage of 15 keV. Beam diameter was between 2 and 5 μm, and ZAF corrections were done. Fe^{2+} and Fe^{3+} were calculated from total Fe measurements on chromites based on the stoichiometric formula of spinels. Several authors (e.g. Wood and Virgo 1989) pointed out that accuracy and precision of such calculations are not

perfect, but precise and accurate enough to obtain reliable Fe^{3+} and Fe^{2+} concentrations. Each grain was measured several times (5–8 spots in the centre) depending on grain size.

Isotope analyses

Whole rock powders were digested in a mixture of concentrated HF and HNO3 in 3-ml screw-top Teflon® vials inside Parr® bombs at ca 180 °C for several days. All samples were spiked with a mixed ^{149}Sm-^{150}Nd tracer prior to dissolution. After complete dissolution, the samples were dried down and re-dissolved in 2.5 N HCl. REE (rare earth elements) were separated using cation exchange columns with a DOWEX AG 50 W-X 12 resin using HCl. Nd and Sm were separated from the other REE using HDEHP-coated Teflon® medium. Sm and Nd were analysed on Re double filaments using a VG-Sector 54 mass spectrometer with multiple collectors (University of Münster, Germany). All Nd isotope ratios were normalised to $^{146}Nd/^{144}Nd = 0.7129$. During the course of this study, the value obtained for the La Jolla Nd-standard was 0.511868 ± 15 (2σ). The uncertainty for the Sm/Nd ratio is ≤0.15 %. The total procedural blank for Nd was <20 pg. Since several 100 ng of Nd were used for an individual isotope analysis, the procedural blank is negligible.

Eight magmatic zircon grains from the gabbro of the southern Sierra de Calalaste were analysed for their U–Pb ages with LA-ICP-MS at the Institut für Mineralogie, Münster. After sieving, the heavy minerals from the <250-µm fraction were separated with a sodium polytungstate solution. Magnetic heavy minerals were removed with a Frantz magnetic separator (only SRT1). A random selection of the total zircon population was mounted in epoxy and polished to expose the centres of the grains. Zircon regions suitable for analysis were identified from CL and backscattered electron imaging. Zircon U–Pb geochronology in Münster was performed using the method outlined in Kooijman et al. (2012). The spot size was 25–35 µm. Total ablation time was 55 s, which included 20 s with the shutter closed to measure the background. Each spot was pre-ablated with three laser shots using a 45-µm beam to remove surface common Pb. External standardisation was done using the GJ-1 reference zircon (Jackson et al. 2004). Measurement of the 91500 standard zircon (Wiedenbeck et al. 1995) as unknown indicated a reproducibility of 2.5 % for $^{206}Pb/^{238}U$ and 3.0 % precision for $^{207}Pb/^{206}Pb$ (2σ). The U and Pb isotope data were processed offline using an in-house Excel® spread sheet (Kooijman et al. 2012). Common-Pb correction was applied if the common ^{206}P of the total ^{206}Pb exceeded 1 % using the Pb evolution model of Stacey and Kramers (1975). Isoplot/Ex 2.49 (Ludwig 2001) was used for age calculations (assuming $\lambda(^{238}U) = 1.551 \times 10^{-10}a^{-1}$ and $\lambda(^{235}U) = 9.849 \times 10^{-10}a^{-1}$; Jaffey et al. 1971) of U–Pb data from zircons of all analysed samples. Three of 35 zircon ages were excluded from further consideration because of large analytical errors.

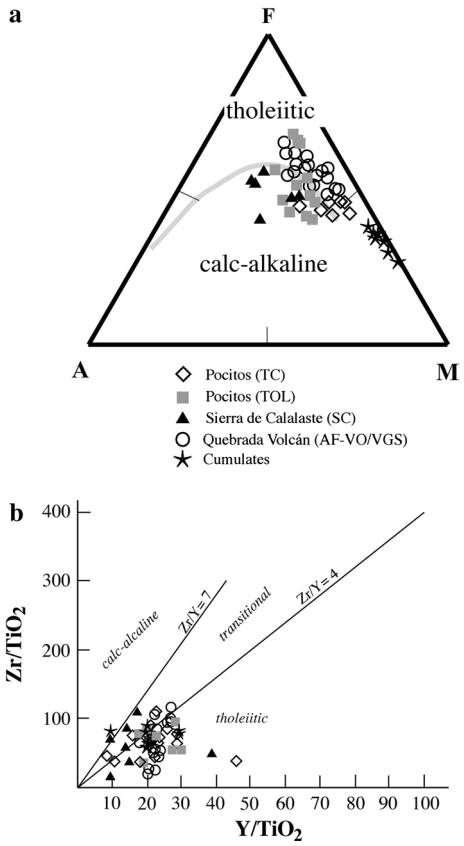

Fig. 3 **a** AFM diagram after Irvine and Baragar (1971). **b** Y/TiO2 versus Zr/TiO2 diagram to discriminate between calc-alkaline and tholeiitic differentiation trends (after Lentz 1998; Piercey et al. 2004)

Geochemistry

Major element geochemistry

The mafic rocks can be classified as gabbros (SiO_2 between 43.1 and 53.1 wt%) and only some as diorites (Table 1 supplementary material), while the ultramafic rocks would be classified as peridotites. The gabbros interlayered with the sedimentary rocks of the Tolillar Formation (Table 1 supplementary material, group TOL; Fig. 2b) show the widest variation in alkali element concentrations between 2.2 and 5.5 wt%. Fe_2O_{3T}, MgO and CaO are variable in each exposure (Table 1 supplementary material). Only Al_2O_3 is significantly lower in the gabbros of the Quebrada Volcán, but the SiO_2 content is generally slightly higher (~50 wt%) than in all other exposures. In an AFM diagram (Fig. 3a).

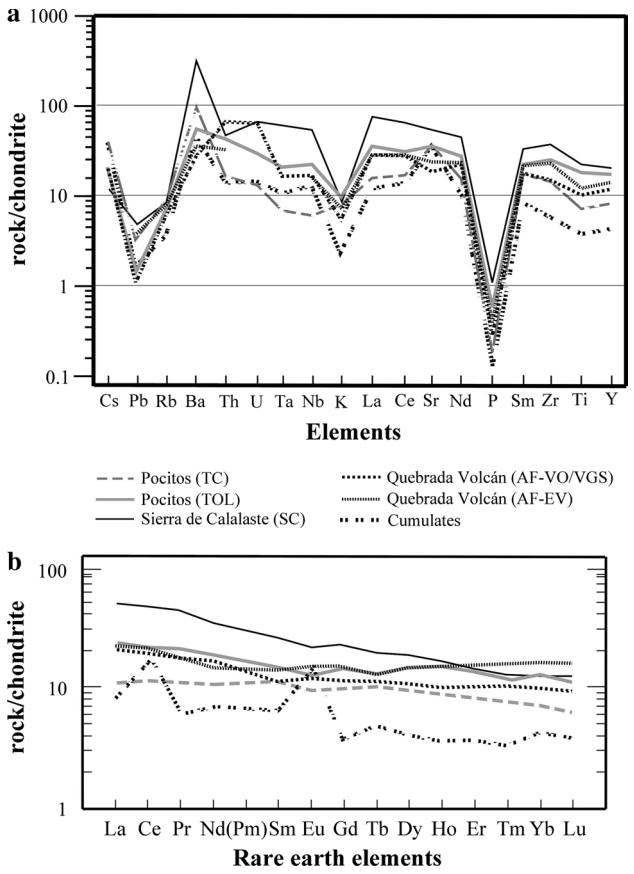

Fig. 4 **a** Samples averages and normalised to chondritic values after Sun and McDonough (1989). **b** Sample averages of rare earth elements normalised to chondritic values after Nakamura (1974)

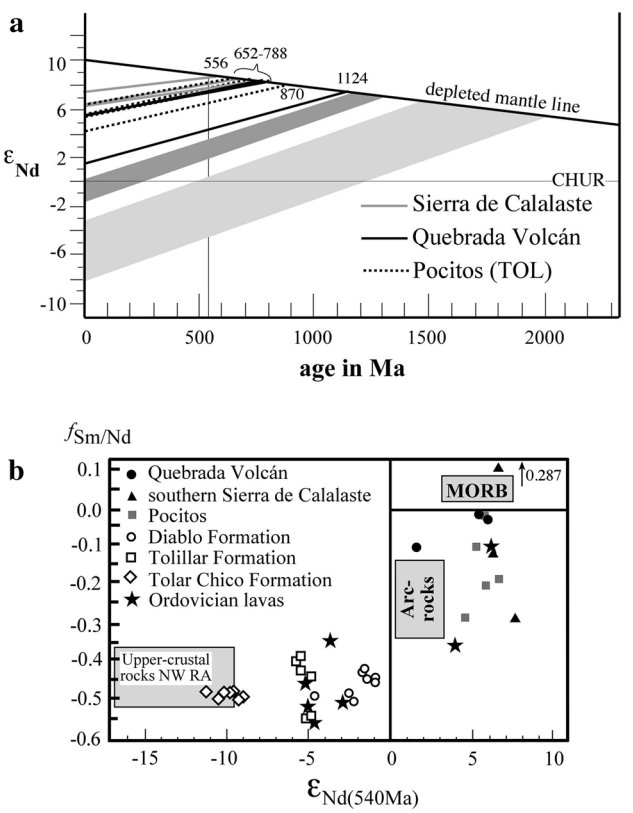

Fig. 5 **a** εNd versus time in Ma. The fine-stippled vertical line represents the crystallisation age of the mafic rocks at 539 Ma, and the data are given for T_{DM} in Ma for the mafic rocks. The *dark-shaded field* represents Nd isotope systematics for arc lavas and the *lighter grey-shaded field* Ordovician sedimentary rocks. **b** Fractionation value for Nd isotopes (*f*) versus εNd values. Shown are Ordovician sedimentary rocks and associated arc lavas and the mafic rocks. The one cumulate sample has the expected high *f* value but its εNd value is similar to the gabbros. Data for Ordovician lavas have been taken from Bock et al. (2000), for the Ordovician sedimentary rocks from Zimmermann and Bahlburg (2003)

most of the rocks follow the tholeiitic trend, but samples of the southern Sierra de Calalaste (SC) seem to be calc-alkaline. Cumulates are depleted in SiO_2, Al_2O_3, TiO_2, alkali elements and strongly enriched in MgO (up to 31 wt%).

Minor and trace element geochemistry

The tholeiitic character of the rocks is better indicated by immobile trace elements in a plot Y/TiO_2 versus Zr/TiO_2 (Fig. 3b). Only few samples fall in a transitional field between tholeiitic and calc-alkaline magmas with Zr/Y ratios between 4 and 7 (Table 1 supplementary material). In extended trace element diagrams, the samples show their general characteristics with relatively uniform enrichment in LILE (large-ion lithophile elements) (Fig. 4a). K_2O is strongly depleted in all samples, as is P_2O_5 and Pb. Incompatible and immobile elements like Th, U, LREE (light rare earth elements) and Zr are mostly enriched. Depletion in Ta, Nb and Ti is weak (Fig. 4a). Some cumulates are significantly different from all other samples and depleted in most of the shown elements, but enriched in compatible elements like Cr, Ni and Co (Table 1 supplementary material data repository). Depletion in incompatible elements such as Zr and Hf is moderate with values 10× higher than chondritic abundances (Fig. 4a; Table 1 supplementary material).

Samples from Pocitos and the Quebrada Volcán show flat REE patterns (Fig. 4b) with La_N/Yb_N ratios mostly between 1 and 3 (Table 1 supplementary material). The samples from Quebrada Volcán close to Antofalla (EV) (Fig. 1c) are enriched in HREE (heavy rare earth elements) relative to others from the same outcrops area at Quebrada Volcán (VO), which have higher SiO_2 contents. The samples from southern Sierra de Calalaste (SC) are partly enriched in LREE, although several samples match the flat REE pattern of the rocks from Pocitos and the Quebrada Volcán. Cumulates have lower REE abundances than the gabbroic rocks with positive Ce and Eu anomalies (Fig. 4b). Chromites from ultramafic rocks show

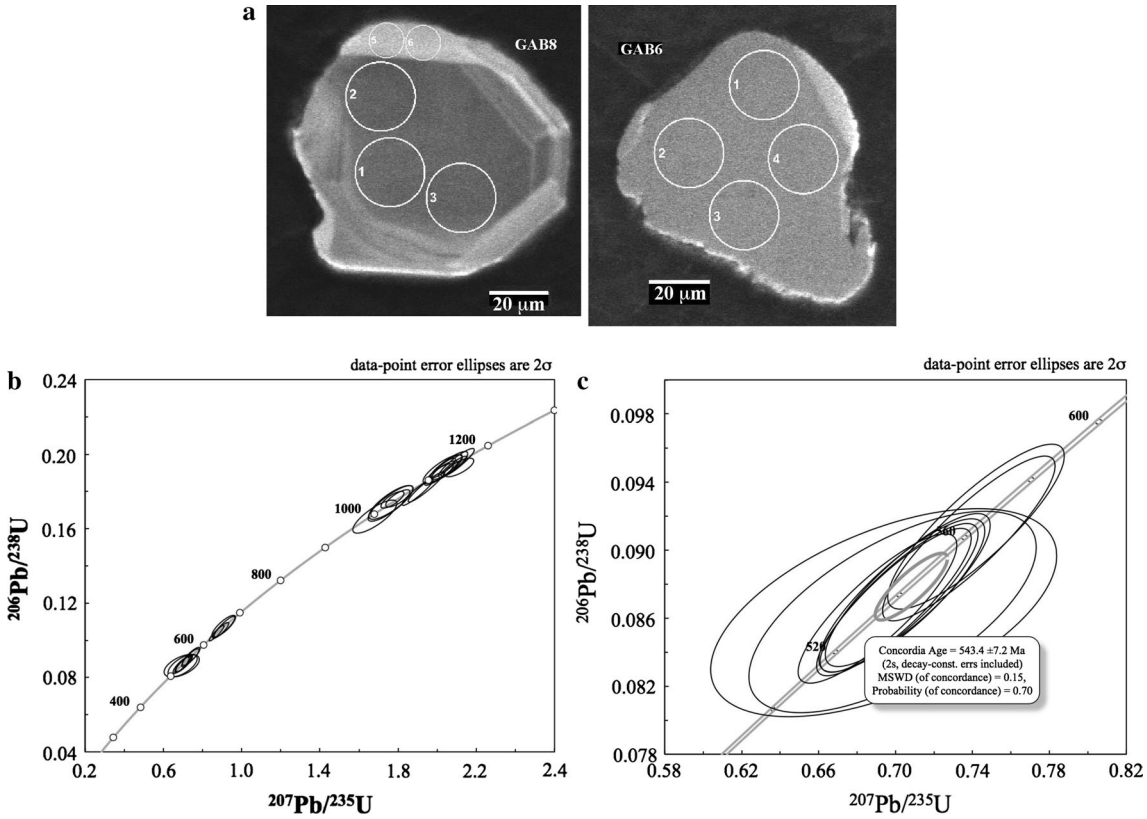

Fig. 6 **a** Representative cathodoluminescence images of zircons GAB8 and GAB6. Spots GAB8-5 and GAB8-6 were analysed with a 25-µm beam, spots 5 and 6 with a 12-µm beam. **b** Weatherill concordia plot of all obtained ages of zircons in the gabbros. **c** Obtained U–Pb ages younger than 600 Ma with nine data points on a Weatherill concordia plot of zircons GAB6 and GAB8

typical Ti, Al, Cr#, Fe^{3+} abundances found in magmatic arc rocks. Low Ce/Pb (<25) and Nb/U (<50) ratios point to a continental rather than an oceanic affinity of the magmas (Hofmann et al. 1986). Most samples have relatively low Y concentrations (±<30 ppm) combined with moderate Cr concentrations (100–400 ppm) and Ni concentrations mostly below 100 ppm, with the exception of gabbros at Pocitos exposed in the Tolar Chico Formation (Table 1 supplementary material). These characteristics do not point to a typical MORB origin.

Isotope geochemistry

Nd isotope compositions

Table 2 presents Nd isotope compositions of gabbroic and cumulate samples with Nd model ages (T_{DM}) and the initial ε_{Nd} based on the youngest magmatic zircon age (c. 540 Ma). In Fig. 5a, εNd_t is plotted against time. The samples have a range of Neoproterozoic Nd model ages (T_{DM}) between 560 and 900 Ma with only one sample having a Mesoproterozoic T_{DM}. Values for εNd_{540Ma} are between +1.4 and +7.4 and are similar to mafic volcanic rocks of Ordovician age in the neighbouring regions of the Cordón de Lila in northern Chile (Fig. 1a) and the eastern Puna of northwestern Argentina (Bock et al. 2000). The positive εNd_t values mark the juvenile character of the mafic rocks. Figure 5b plots $f_{Sm/Nd}$ values against $\varepsilon Nd_{t=540Ma}$. The diagram shows that the degree of fractionation or assimilation of crustal material varies between the gabbroic samples.

Geochronology

U–Pb ages of magmatic zircon

From the gabbroic rocks, magmatic zircon grains could be separated for U–Pb age determination by LA-ICP-MS. The zircons are small (<150 µm), slightly rounded and partly broken (Fig. 6a). Thirty ages with very good to acceptable σ errors could be obtained from the zoned zircon grains, and they range from 1,182 ± 39 to 534 ± 29 Ma (Fig. 6b; Table 1). The eight analysed zircon grains gave four groups of ages centreed at 1,130, 1,020, 650 and 540 Ma (Fig. 6c; Table 1). Of particular interest regarding the age of the

Table 1 U–Pb isotope data from primary and inherited zircons in gabbros

Analysis name	Spot	U conc. (ppm)	Ratios						Rho
			$^{206}Pb/^{238}U$	$\pm2\sigma$	$^{207}Pb/^{235}U$	$\pm2\sigma$	$^{206}Pb/^{238}U$	$\pm2\sigma$	
GAB8-5-12	Rim	237	0.0863	0.0050	0.6938	0.0735	0.0583	0.0052	0.55
GAB8-6-12	Rim	236	0.0864	0.0048	0.6985	0.0610	0.0587	0.0039	0.64
GAB8-3-25	Core	271	0.0866	0.0036	0.6906	0.0337	0.0579	0.0015	0.85
GAB8-2-25	Core	285	0.0870	0.0035	0.6992	0.0329	0.0583	0.0014	0.87
GAB8-1-25	Core	330	0.0872	0.0036	0.7019	0.0335	0.0584	0.0014	0.86
GAB6-2-25	Rim	198	0.0873	0.0037	0.7033	0.0352	0.0584	0.0016	0.84
GAB6-4-25	Core	159	0.0877	0.0037	0.7063	0.0350	0.0584	0.0015	0.85
GAB6-3-25	Rim	221	0.0907	0.0040	0.7381	0.0366	0.0590	0.0014	0.88
GAB6-1-25	Rim	184	0.0914	0.0040	0.7418	0.0375	0.0589	0.0015	0.86
GAB5-2-25	Core mm	369	0.1038	0.0034	0.8722	0.0311	0.0609	0.0009	0.92
GAB5-1-25	Core mm	232	0.1053	0.0035	0.8932	0.0339	0.0615	0.0011	0.88
GAB5-4-25	Rim mm	371	0.1073	0.0045	0.9130	0.0438	0.0617	0.0014	0.88
GAB5-3-25	Core mm	365	0.1075	0.0048	0.9085	0.0495	0.0613	0.0019	0.82
GAB2-1-25	Metamict	142	0.1417	0.0042	1.4494	0.0561	0.0742	0.0018	0.77
GAB7-3-25	Core	120	0.1665	0.0073	1.6812	0.0920	0.0732	0.0024	0.80
GAB7-2-25	Core	86	0.1736	0.0078	1.7617	0.0943	0.0736	0.0021	0.84
GAB7-1-25	Core	101	0.1741	0.0074	1.7625	0.0920	0.0734	0.0022	0.82
GAB7-4-25	Core	228	0.1750	0.0086	1.7765	0.1011	0.0736	0.0021	0.86
GAB2-3-25	Rim mm	206	0.1756	0.0037	1.7711	0.0482	0.0732	0.0013	0.77
GAB2-2-25	mm Core	176	0.1763	0.0038	1.7987	0.0507	0.0740	0.0014	0.76
GAB4-1-25	Rim mm	262	0.1795	0.0058	1.8993	0.0653	0.0767	0.0009	0.93
GAB4-2-25	Core mm	262	0.1824	0.0067	1.9430	0.0752	0.0773	0.0010	0.94
GAB1-3-25	1st Rim	165	0.1898	0.0042	2.0139	0.0553	0.0770	0.0012	0.81
GAB1-2-25	Core-Rim	256	0.1916	0.0040	2.0389	0.0543	0.0772	0.0013	0.79
GAB4-3-25	Core-Rim mm	215	0.1916	0.0067	2.0312	0.0787	0.0769	0.0013	0.91
GAB3-3-25	Rim mm	82	0.1920	0.0063	2.0275	0.0816	0.0766	0.0018	0.82
GAB1-5-25	1st Rim	267	0.1927	0.0043	2.0305	0.0522	0.0764	0.0010	0.87
GAB1-1-25	Core	149	0.1929	0.0041	2.1117	0.0613	0.0794	0.0016	0.73
GAB3-2-25	1st Rim mm	102	0.1935	0.0066	2.0568	0.0810	0.0771	0.0015	0.86
GAB1-4-25	Core	270	0.1935	0.0045	2.0853	0.0537	0.0782	0.0009	0.89
GAB3-1-25	Core mm	150	0.1954	0.0063	2.0979	0.0748	0.0779	0.0012	0.91

Analysis name	Spot	Ages (Ma)						Common Pb		Degree of concordance (%)
		$^{206}Pb/^{238}U$	$\pm2\sigma$	$^{207}Pb/^{235}U$	$\pm2\sigma$	$^{207}Pb/^{206}Pb$	$\pm2\sigma$	$^{206}Pb/^{204}Pb$	$f206$ %	
GAB8-5-12	Rim	533.8	29.7	535.1	44.1	540.8	194.9	*		98.7
GAB8-6-12	Rim	534.0	28.7	537.9	36.5	554.3	146.6	1,249	1.09	96.3
GAB8-3-25	Core	535.2	21.3	533.2	20.3	524.5	56.6	7,557	0.05	102.0
GAB8-2-25	Core	537.5	21.0	538.3	19.6	541.9	51.3	*		99.2
GAB8-1-25	Core	538.9	21.2	539.9	20.0	544.1	53.8	134,998	0.01	99.1
GAB6-2-25	Rim	539.8	21.8	540.8	21.0	544.8	59.3	*		99.1
GAB6-4-25	Core	541.6	21.8	542.6	20.8	546.5	57.8	*		99.1
GAB6-3-25	Rim	559.6	23.4	561.3	21.4	568.2	51.3	*		98.5
GAB6-1-25	Rim	563.7	23.4	563.5	21.9	562.5	56.6	*		100.2
GAB5-2-25	Core mm	636.7	19.8	636.7	16.9	636.8	30.9	20,995	0.06	100.0
GAB5-1-25	Core mm	645.2	20.6	648.1	18.2	657.9	38.0	*		98.1
GAB5-4-25	Rim mm	657.1	26.5	658.6	23.2	664.0	48.0	*		98.9
GAB5-3-25	Core mm	658.4	28.0	656.3	26.3	649.1	66.8	6,386	0.18	101.4

Table 1 continued

Analysis name	Spot	Ages (Ma)						Common Pb		Degree of concordance (%)
		$^{206}Pb/^{238}U$	$\pm 2\sigma$	$^{207}Pb/^{235}U$	$\pm 2\sigma$	$^{207}Pb/^{206}Pb$	$\pm 2\sigma$	$^{206}Pb/^{204}Pb$	$f206$ %	
GAB2-1-25	Metamict	854.1	24.0	909.6	23.3	1,047.0	49.4	3,226	0.42	81.6
GAB7-3-25	Core	992.8	40.2	1,001.4	34.8	1,020.4	66.8	*		97.3
GAB7-2-25	Core	1,031.9	43.0	1,031.5	34.7	1,030.6	58.5	1,732	0.44	100.1
GAB7-1-25	Core	1,034.8	40.8	1,031.8	33.8	1,025.3	61.0	1,957	0.45	100.9
GAB7-4-25	Core	1,039.7	47.0	1,036.9	37.0	1,031.0	58.6	*		100.8
GAB2-3-25	Rim mm	1,042.8	20.2	1,034.9	17.6	1,018.3	35.1	5,287	0.18	102.4
GAB2-2-25	mm Core	1,046.8	20.7	1,045.0	18.4	1,041.2	36.9	*		100.5
GAB4-1-25	Rim mm	1,064.5	31.5	1,080.9	22.9	1,114.0	24.6	*		95.6
GAB4-2-25	Core mm	1,080.2	36.3	1,096.0	26.0	1,127.8	25.7	4,154	0.19	95.8
GAB1-3-25	1st Rim	1,120.2	22.9	1,120.2	18.6	1,120.2	32.2	7,173	0.07	100.0
GAB1-2-25	Core-Rim	1,129.7	21.9	1,128.6	18.1	1,126.4	32.3	*		100.3
GAB4-3-25	Core-Rim mm	1,130.1	36.5	1,126.0	26.4	1,118.1	32.5	3,739	0.44	101.1
GAB3-3-25	Rim mm	1,132.0	34.2	1,124.8	27.4	1,110.9	46.3	*		101.9
GAB1-5-25	1st Rim	1,135.7	23.2	1,125.8	17.5	1,106.6	25.6	6,041	0.27	102.6
GAB1-1-25	Core	1,137.3	22.0	1,152.6	20.0	1,181.6	39.4	17,081	0.08	96.3
GAB3-2-25	1st Rim mm	1,140.2	35.4	1,134.6	26.9	1,123.7	39.8	6,380	0.12	101.5
GAB1-4-25	Core	1,140.2	24.1	1,144.0	17.7	1,151.1	22.8	*		99.1
GAB3-1-25	Core mm	1,150.6	34.1	1,148.1	24.5	1,143.5	29.8	1,649	0.98	100.6

* No detectable ^{204}Pb

gabbros is the youngest age group. It is represented by zircon grains GAB8 and GAB6, which provided nine concordant $^{206}Pb/^{238}U$–$^{207}Pb/^{235}U$ ages (Fig. 6c), seven from the cores and two from the rim of zircon GAB8. These two rim spots were measured with a 12-μm-diameter beam and consequently have slightly increased errors. All dates from zircon grains GAB8 and GAB6 combinedly define a concordia age of 543.4 ± 7.2 Ma (Fig. 6c). The weighted average age of these analyses is 542.9 ± 7.5 Ma (MSWD = 0.87, probability of fit = 0.54).

The concordia age of 543.4 ± 7.2 Ma is interpreted as the intrusion age. This interpretation is based on two independent lines of evidence. First, the rims and cores of zircon grains GAB8 and GAB6 have a similar age. Second, the contact of the Puna ultramafic rocks and gabbros (Complejo Ojo de Colorados, Zappettini et al. 1994) to early Ordovician monzonites and monzodiorites of the Complejo Ígneo Pocitos is marked by a black wall characterised by low initial $^{87}Sr/^{86}Sr$ values (Kleine et al. 2004). They indicate that gabbros and ultramafic rocks originated in a continental crust significantly older than the intrusion age of the Ordovician plutons at 476 ± 2 Ma (Kleine et al. 2004).

The presented analyses are the first and only reliable ages on zircon available for the mafic–ultramafic assemblage of the Complejo Ojo de Colorados, and the first hard evidence constraining its age. An age of c. 545 Ma corresponds to the lowermost Cambrian to Ediacaran and connects the intrusive bodies to the Pampean orogeny, which took place between 555 and 520 Ma (Rapela et al. 1998; Schwartz et al. 2008). It establishes the dated rocks as a temporal equivalent to the late stages of the evolution of the western margin of the Pampia terrane, including the Puncoviscana basin (see summary of ages in Augustsson et al. 2011).

Discussion

The rocks of the mafic complexes at Pocitos, in the Sierra de Calalaste and the Quebrada Volcán in NW Argentina have a predominantly tholeiitic character (Fig. 3). The gabbroic rocks show mostly enrichment in Zr and other incompatible elements, and moderate depletions in Ta, Nb and Ti (Fig. 4a; Table 1 supplementary material). This indicates a noteworthy crustal contamination, as the rocks are not significantly fractionated (Fig. 4b). Comparing the geochemistry of the rocks with typical mid-ocean ridge basalts (MORB), an extended trace element diagram shows that the samples are not similar to MORBs (Fig. 7a). The mafic rocks exposed in the Central Andes are enriched in LILE, Th, Ta, Nb, LREE, Hf and Ti compared to MORB. Ce/Nb and Th/Nb ratios are atypical for MORB and

might point either to partially crustal contaminated rocks or reflect elemental enrichment in their magmatic source (Fig. 7). Some samples of the southern Sierra de Calalaste have partly higher Nb concentrations, while Ce increases only slightly (by factor 2) and Th is very similar to concentrations in the other gabbros (see Figs. 4a, 7a; Table 1 supplementary material). However, still none of the samples points to a typical MORB source. The abundance of primary magmatic hornblende does also not support an MORB origin. Moreover, we identified chromite in olivines of the cumulate rocks at Pocitos with chemical signatures typical of arc magmas with Ti_2O between 0.84 and 0.99 %, low Al_2O_3 (6.2–7.8 %), high Cr# (0.89–0.90) and high Fe^{3+} values (0.14–0.39) (Arai 1992; Kamenetsky et al. 2001). Neodymium isotope systematics demonstrate the juvenile character of the rocks with Late Neoproterozoic T_{DM}, except for one sample with a Mesoproterozoic model age, when using the age of the youngest zircon separated from the gabbros for the calculation of T_{DM}. The dated zircons are slightly rounded, and 6 out of 8 grains are considered inherited from crustal rocks because of their Meso- and Neoproterozoic ages. The spread of the initial Nd isotope ratios, however, is low and indicates that crustal contamination, although present, might not have been a major factor in the evolution of the magmas from which the gabbros crystallized.

The dated gabbros are tectonically associated with Ordovician clastic successions, which are part of a wide marine retro-arc basin stretching from the west in northern Chile to the east in the Argentinean Cordillera Oriental (Fig. 1a). The sedimentary rocks were subject of c. 20-year-long provenance studies (Bahlburg 1990, 1998; Bock et al. 2000; Zimmermann et al. 2002, 2010; Zimmermann and Bahlburg 2003) and revealed not a single argument for a possible terrane boundary in that area marked by the mafic to ultramafic rocks. The clastic Ordovician successions comprise Nd isotope systematics similar to the underlying metamorphic basement and revealed crustal reworking without significant input of juvenile material, (Zimmermann and Bahlburg 2003), which was also revealed in Ordovician continental arc-related lavas and plutonic rocks (Bock et al. 2000; Kleine et al. 2004; Poma et al. 2004). Detrital zircon analyses of the Ordovician sedimentary rocks hosting the gabbros show an overwhelming abundance of Ordovician detrital zircons (Naidoo et al. 2012). About 90 % of the detrital zircons in these successions are younger than 520 Ma (Naidoo et al. 2012) and can be assigned to the active continental margin lasting from Late Cambrian to Middle Ordovician (Bahlburg 1990; Mannheim and Miller 1996; Pankhurst et al. 1998; Zimmermann and Bahlburg 2003; Zimmermann et al. 2010); other ages are extremely rare even those corresponding to the Early to Middle Cambrian Pampeanas

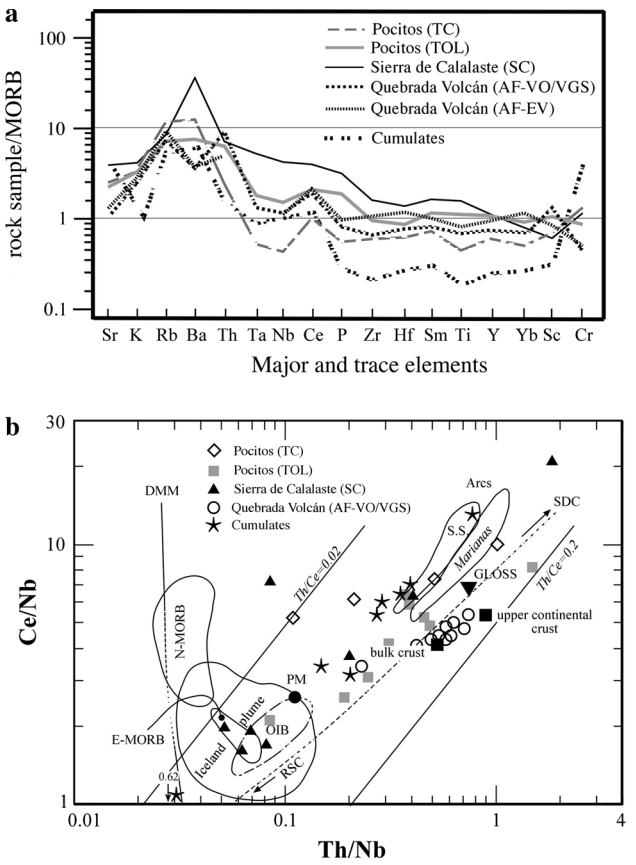

Fig. 7 **a** Normalisation of sample averages to MORB after Pearce (1983). **b** Discrimination plot for basaltic magmas and their genesis after Wang et al. (2004)

orogeny. Moreover, the host rocks of the gabbros represent the top of a sedimentary package with a minimum thickness of 3 km (Zimmermann 1999; Zimmermann et al. 2002). Field studies demonstrated that despite detailed mapping over several km^2 (Fig. 1 repository material), no xenoliths from intermediate to felsic magmatic rocks or sedimentary successions could be found in the mafic bodies. Sedimentary rocks show mylonitic textures along the contacts or 1–2-m-wide talc-rich contact zones. The gabbroic rocks are exposed as elongated lenses in various different levels of the sedimentary rocks (Fig. 1 supplementary material). Moreover, the metamorphic grade of the mafic rocks as indicated by new growth of chlorite, serpentine and amphibole is definitely higher than that of the associated sedimentary successions, which were affected only by diagenetic to anchimetamorphic conditions (Zimmermann 1999; Zimmermann and Bahlburg 2003). In view of the field evidence, contamination by the supracrustal Ordovician rocks during intrusion should reveal a dominance of Ordovician zircons. However, this is not observed. The zircons studied here have Mesoproterozoic, Early Ediacaran and Early Cambrian core and rim ages

Table 2 Nd isotope geochemical data for the mafic rocks

Sample	Rock type	Exposure	Age (Ma)	Sm (ppm)	Nd (ppm)	$^{147}Sm/^{144}Nd$	$^{143}Nd/^{144}Nd$	$^{143}Nd/^{144}Nd_i$	$\varepsilon Nd_{t=540}$	T_{DM} (Ma)	f
EV13	Gabbro	Quebrada Volcán/Antofalla	540	3.35	11.51	0.1759	0.512640	0.512018	1.5	1,124	−0.106
EV11	Gabbro	Quebrada Volcán/Antofalla	540	4.10	12.73	0.1950	0.512909	0.512219	5.4	763	−0.009
EV10	Gabbro	Quebrada Volcán/Antofalla	540	2.94	9.34	0.1899	0.512901	0.512229	5.6	743	−0.035
Poc 5-5	Gabbro	Pocitos	540	6.61	28.51	0.1402	0.512658	0.512162	4.3	870	−0.287
A 272	Gabbro	Pocitos	540	2.95	11.36	0.1570	0.512831	0.512276	6.5	652	−0.202
A 220-6	Gabbro	Pocitos	540	2.70	10.49	0.1556	0.512789	0.512238	5.8	725	−0.209
A4-6	Gabbro	Pocitos	540	4.48	13.82	0.1960	0.512913	0.512220	5.4	762	−0.004
A 4-4	Gabbro	Pocitos	540	1.64	5.64	0.1758	0.512828	0.512206	5.1	788	−0.106
C 15	Gabbro	Southern Calalaste	540	7.42	31.62	0.1419	0.512824	0.512322	7.4	556	−0.279
C 62	Gabbro	Southern Calalaste	540	7.80	27.51	0.1714	0.512866	0.512260	6.2	684	−0.129
C 137	Cumulate	Southern Calalaste	540	0.67	1.60	0.2532	0.513171	0.512275	6.5	652	0.287

Model ages are calculated after DePaolo (1981)

(Table 1) indicating that the magmas assimilated Meso- and Neoproterozoic crustal material prior to final intrusion at c. 545 Ma, i.e. at the boundary Pre-Cambrian–Cambrian.

Conclusion

Mafic to ultramafic rocks formed at c. 545 Ma are exposed in northwest Argentina in tectonic contact with Ordovician sedimentary successions. This study shows that the mafic to ultramafic suite is mainly composed of tholeiitic to calc-alkaline gabbros, which are affected by hydrothermal processes and witnessed new growth of epidote, chlorite, pumpellyite, biotite, serpentine and amphibole, which is not recorded in the host rocks and points to a higher metamorphic grade. Most of the mafic rocks are enriched in LILE elements and display a slight negative anomaly in Ta, Nb and partly Ti compared to chondrites (Fig. 4a). However, compared to MORB, the rocks are enriched in incompatible elements particularly LILE (Fig. 7a). Cumulates occur in the suite of mafic rocks and contain chromite with chemical signatures pointing to arc magmas. Neodymium model ages (T_{DM}) are mostly Neoproterozoic (Table 2; Fig. 5a). The gabbros contain primary zircon grains giving an age of 543.4 ± 7.2 Ma and inherited zircon of Mesoproterozoic and Ediacaran age (Table 1; Fig. 6c). Models presented by a number of studies (Dalziel and Forsythe 1985; Palma et al. 1990; Rapela et al. 1992; Forsythe et al. 1993; Blasco et al. 1996; Conti et al. 1996; Ramos 1988, 1996; Rapalini 2005; Ramos 2008) interpreting the rock suite as Ordovician MORB have to be considered unlikely because they imply (1) young Neodymium model ages (T_{DM}) and (2), this is a defining argument, the absence of inherited zircon crystals. These two major criteria for MORB could not be identified in our study.

The formation of the gabbros and the associated ultramafic rocks in the southern Argentine Puna was related to the evolution of the active western margin of the Pampia terrane, including the Puncoviscana basin, during the Late Neoproterozoic and earliest Cambrian. In contrast to previous interpretations, the rocks are recognised to predate the Ordovician evolution of the Central proto-Andean active margin. Consequently, interpretations and palaeotectonic reconstructions assuming these rocks to represent an oceanic terrane suture of Ordovician age have to be dismissed.

Acknowledgments The studies of UZ and HB were funded by Deutsche Forschungsgemeinschaft grant Ba 1011/8-1 and the University of Stavanger. We thank F. Hongn, Salta, for many discussions during the progress of this study. C. Franzen and C. Huck are thanked for company during fieldwork. Lisa Jean Bingham is thanked for help with the use of GIS application for Fig. 1 supplementary material. Constructive and thoughtful reviews by F. Lucassen and C. Cingolani are gratefully acknowledged.

References

Aalto KR (1982) The Franciscan complex of northernmost California: sedimentation and tectonics. In: Leggett JK (ed) Trench-Forearc geology. Geol Soc Lond Spec Publ 10:419–432

Allmendinger RW, Jordan TE, Palma M, Ramos VA (1982) Perfil estructural en la Puna Catamaqueña (25°–27°S), Argentina. V Congr Latinoam Geol Actas I:499–518

Arai S (1992) Chemistry of chromian spinel in volcanic rocks as a potential guide to magma chemistry. Miner Mag 56:173–184

Argañaraz R, Viramonte J, Salazar L (1973) Sobre el hallazgo de serpentinitas en la Puna Argentina. V Congr Geol Argent Actas I:23–32

Augustsson C, Rüsing T, Adams CJ, Zimmermann U, Chmiel H, Kocabayoğlu M, Büld M, Zimmermann U, Berndt J, Kooijman E (2011) Detrital quartz and zircon combined: the production of mature sand with short transportation paths along the Cambrian West Gondwana margin, NW Argentina. J Sed Res 81:284–298

Bahlburg H (1990) The Ordovician basin in the Puna of NW Argentina and N Chile: geodynamic evolution from back-arc to foreland basin. Geotekton Forsch 75:1–107

Bahlburg H (1998) The geochemistry and provenance of Ordovician turbidites in the Argentine Puna. In: Pankhurst RJ, Rapela CW (eds) The Proto-Andean Margin of Gondwana. Geol Soc Lond Spec Publ 142:127–142

Bahlburg H, Hervé F (1997) Geodynamic evolution and tectonostratigraphic terranes of northwestern Argentina and northern Chile. Geol Soc Am Bull 109:869–884

Bahlburg H, Vervoort JD, Du Frane SA, Bock B, Augustsso C (2009) Timing of crust formation and recycling in accretionary orogens: the detrital zircon U–Pb and Hf, and the whole-rock Nd isotope evidence of Devonian to Permian turbidite deposits of the Gondwana margin in northern Chile. Earth Sci Rev 97:215–241

Blasco G, Villar L, Zappettini EO (1996) El complejo ofiolítico desmembrado de la Puna argentina, Provincias de Jujuy, Salta y Catamarca. XIII Congr Geol Argent y III Congr Expl Hidrocarb Actas III: 653–667

Bock B, Bahlburg H, Wörner G, Zimmermann U (2000) Tracing crustal evolution in the southern central Andes from the Late Precambrian to Permian with Geochemical and Nd and Pb isotope data. J Geol 108:515–535

Coira B (1974) Levantamiento de la hoja 9°-b, Salar de Antofalla, provincia de Catamarca. Serv Geol Nac (unpublished report)

Coira BL, Kay SM, Peréz B, Woll B, Hanning M, Flores P (1999) Magmatic sources and tectonic setting of Gondwana margin Ordovician magmas, northern Puna of Argentina and Chile. In: Ramos VA, Keppie JD (eds) Laurentia-Gondwana connection before Pangea. Geol Soc Am Spec Paper 336:145–170

Coira B, Kirschbaum A, Hongn F, Pérez B, Menegatti N (2009a) Basic magmatism in northeastern Puna, Argentina: chemical composition and tectonic setting in the Ordovician back-arc. J S Am Earth Sci 27:374–382

Coira B, Koukharsky M, Ribeiro Guevara S, Cisterna CE (2009b) Puna (Argentina) and northern Chile Ordovician Basic magmatism: a contribution to the tectonic setting. J S Am Earth Sci 27:24–35

Conti CM, Rapalini AE, Coira B, Koukharsky M (1996) Palaeomagnetic evidence of an early Palaeozoic rotated terrane in Northwest Argentina; a clue for Gondwana-Laurentia interaction? Geology 24:953–956

Dalziel IWD, Forsythe RD (1985) Andean evolution and the terrane concept. In: Howell DG (ed) Tectonostratigraphic terranes of the Circum-Pacific Region. Circum-Pacific-Council Energ Miner Resourc Earth Sci Ser 1:565–581

DePaolo DJ (1981) Trace element and isotopic effects of combined wallrock assimilation and fractional crystallisation. Earth Plan Sci Lett 53:189–202

Dilek Y, Newcomb S (eds) (2003) Ophiolite concept and the evolution of geological thought. Geol Soc Am Spec Paper 373:1–504

Egenhoff SO (2007) Life and death of a Cambrian-Ordovician basin: an Andean three act play featuring Gondwana and the Arequipa-Antofalla terrane. Geol Soc Am Spec Paper 423:511–524

Egenhoff SO, Lucassen F (2003) Chemical and isotopic composition constrain the source of lower to upper Ordovician sediments from the Andes of south Bolivia. J Geol 111:487–497

Forsythe RD, Davidson J, Mpodozis C, Jesinkey C (1993) Lower Palaeozoic relative motion of the Arequipa block and Gondwana: palaeomagnetic evidence from Sierra de Almeida of northern Chile. Tectonics 12:219–236

Hall J (1865) Figures and descriptions of Canadian organic remains; Decade II, graptolites of the Quebec group. Geol Surv Can 1–151

Hofmann AW, Jochum KP, Seufert M, White WM (1986) Nb and Pb in oceanic basalts; new constraints on mantle evolution. Earth Plan Sci Lett 79:33–45

Howell DG, Jones DL, Schermer ER (1985) Tectonostratigraphic terranes of the Circum-Pacific Region. In: Howell DG (ed) Tectonostratigraphic terranes of the Circum-Pacific Region. Circum-Pacific-Council Energ Miner Resourc Earth Sci Ser 1:3–30

Irvine TN, Baragar WRA (1971) A guide to the chemical classification of the common volcanic rocks. Can J Earth Sci 8:523–548

Jackson SE, Pearson NJ, Griffin WL, Belousova EA (2004) The application of laser ablation-inductively coupled plasma-mass spectrometry to in situ U–Pb zircon geochronology. Chem. Geol. 211:47–69

Jaffey AH, Flynn KF, Glendenin LE, Bentley WC, Essling AM (1971) Precision measurements of half-lives and specific activities of 235U and 238U. Phys Rev C 4:1889–1906

Kamenetsky VS, Crawford AJ, Meffre S (2001) Factors controlling chemistry of magmatic spinel: an empirical study of associated olivine, Cr-spinel and melt inclusions from primitive rocks. J Petrol 42:655–671

Kay SM, Maksaev V, Mpodozis C, Moscoso R, Nasi C (1987) Probing the evolving Andean lithosphere: middle to late tertiary magmatic rocks in Chile over the modern zone of subhorizontal subduction (29°–31.5°S). J Geophys Res 92:6173–6189

Keppie JD (1989) Northern Appalachian terranes and their accretionary history. Geol Soc Am Spec Paper 230:159–192

Kleine T, Mezger K, Münker K, Zimmermann U, Bahlburg H (2004) Crustal evolution along the Early Ordovician proto-Andean margin of Gondwana: trace element and isotope evidence from the Complejo Ígneo Pocitos (NW Argentina). J Geol 112:503–520

Kooijman E, Berndt J, Mezger K (2012) U–Pb dating of zircon by laser ablation ICP-MS: recent improvements and new insights. Eur J Min 24:5–21

Lentz DR (1998) Petrogenetic evolution of felsic volcanic sequences associated with Phanerozoic volcanic-hosted massive sulfide systems: the role of extensional geodynamics. Ore Geol Rev 12:289–327

Lindholm K (1991) Ordovician graptolites from the early Hunneberg of southern Scandinavia. Palaeontology 34:283–327

Lucassen F, Becchio R, Wilke HG, Franz G, Thirwall MF, Viramonte J, Wemmer K (2000) Proterozoic–Palaeozoic development of the basement of Central Andes (18–26°)—a mobile belt of the South American craton. J S Am Earth Sci 13:697–715

Lucassen F, Franz G, Romer RL, Schultz F, Dulski P, Wemmer K (2007) Pre-Cenozoic intra-plate magmatism along the Central Andes (17–34°S): composition of the mantle at an active margin. Lithos 99:312–338

Mannheim R, Miller H (1996) Las rocas volcánicas y subvolcánicas eopaleozoicas del Sistema de Famatina. Münch Geol Hefte A 19:159–186

Mantle GW, Collins WJ (2008) Quantifying crustal thickness variations in evolving orogens: correlation between arc basalt composition and Moho depth. Geology 36:87–90

Martos DE (1982) Estadística y correlación geoquímica en la región de Antofalla, Província de Catamarca. V Congr Latinoamér Geol Actas IV:147–157

Mon R, Hongn F (1991) The structure of the Precambrian and lower Palaeozoic basement of the Central Andes between 22° and 32° Lat. Geol Rundsch 80:745–758

Naidoo T, Zimmermann U, Vervoort J (2012) Detrital zircon provenance of late ordovician to early silurian successions in Northwest Argentina. Vinterkonferansen 2011, Norsk Geologisk Forening NGF Abstracts and Proceedings 1:68–69

Nakamura N (1974) Determination of REE, Ba, Fe, Mg, Na, and K in carbonaceous and ordinary chondrites. Geochim Cosmoch Acta 38:57–775

Palma MA, Brisson I, Vujovich G (1990) Geológia del bloque de la Quebrada Honda, Puna Cartamarqueña. Rev Assoc Geol Arg 45:145–158

Pankhurst RJ, Rapela CW, Saavedra J, Baldo E, Dahlquist J, Pascua I, Fanning CM (1998) The Famatinian magmatic arc in the central Sierras Pampeanas: an Early to Mid Ordovician continental arc on the Gondwana margin. In: Pankhurst RJ, Rapela CW (eds) The Proto-Andean Margin of Gondwana. Geol Soc Lond Spec Publ 142:181–217

Pearce JA (1983) Role of the sub-continental lithosphere in magma genesis at active continental margins. In: Hawkesworth CJ, Norry MJ (eds) Continental basalts and mantle xenoliths. Shiva, Nantwich, pp 230–249

Piercey SJ, Murphy DC, Mortensen JK, Creaser RA (2004) Mid-Palaeozoic initiation of the northern Cordilleran marginal backarc basin: geologic, geochemical, and neodymium isotope evidence from the oldest mafic magmatic rocks in the Yukon-Tanana terrane, Finlayson Lake district, southeast Yukon, Canada. Geol Soc Am Bull 116:1087–1106

Poma S, Quenardelle S, Litvak V, Maisonnave EB, Koukharsky M (2004) The Sierra de Macon, Plutonic expression of the Ordovician magmatic arc, Salta Province Argentina. J S Am Earth Sci 16:587–597

Quenardelle S, Poma S (2008) Quebrada Tramontana (Sierra De Calalaste): evidencias de metamorfismo térmico en caja de rocas ultramáficas. XVII Congr Geol Argent Actas II:675–676

Ramos VA (1988) Late Proterozoic-Early Palaeozoico of South America—a collisional history. Episodes 11:168–174

Ramos VA (1996) Evolución de la plataforma continental. In: Ramos VA, Turic MA (Eds) Geología y recursos naturales de la plataforma continental Argentina. XIII Congr Geol Argent y III Congr Explor Hidrocarb Relatorio 385–404

Ramos VA (1999) Las provincias geológicas del territorio Argentino. In: Caminos R (ed) Geología Argentina. SEGEMAR 29:41–95

Ramos VA (2008) The basement of the Central Andes: the Arequipa and related terranes. Ann Rev Earth Plan Sci 36:289–324

Ramos VA, Vujovich G, Martion R, Otamendi J (2010) Pampia: a large cratonic block missing in the Rodinia supercontinent. J Geodyn 50:243–255

Rapalini AE (2005) The accretionary history of southern South America from the latest Proterozoic to the late Palaeozoic: some Palaeomagnetic constraints. In: Vaughan APM, Leat PT, Pankhurst RJ (eds) Terrane processes at the Margins of Gondwana. Geol Soc Lond Spec Publ 246:305–328

Rapela CW, Coira B, Toselli A, Saavedra J (1992) El magmatismo del Paleózoico en el Sudoeste de Gondwana. In: Gutiérrez Marco JG, Saavedra J, Rábano I (eds) Palaeozóico Inferior de Ibero-América. IUGS Series 21–68

Rapela CW, Pankhurst RJ, Casquet C, Baldo E, Saavedra J, Galindo C, Fanning CM (1998) The Pampean Orogeny of the southern proto-Andes: Cambrian continental collision in the Sierras de Cordoba. In: Pankhurst RJ, Rapela CW (eds) The Proto-Andean Margin of Gondwana. Geol Soc Lond Spec Publ 142:181–217

Robertson AHF, Xenophontos C (1997) Cyprus. In: Eldridge Moores M, Fairbridge RW (eds) Encyclopedia of European and Asian regional geology, pp 160–171

Schwartz JJ, Gromet LP, Miró R (2008) Timing and duration of the calcalcaline arc of the Pampean Orogeny: implications for the Late Neoproterozoic to Cambrian evolution of Western Gondwana. J Geol 116:39–61

Seggiaro R, Becchio R (1999) Inversión Tectónica en la Sierra Quebrada Honda. Puna Austral. Catamarca-Argentina. IX Congr. Geol. Chile Actas I:25–26

Seggiaro R, Hongn F, Folguera A, Clavero J (2002) Mapa geológico de la Hoja 2769 II. Paso de San Francisco, Escala 1:250.000. SEGEMAR

Stacey JS, Kramers JD (1975) Approximation of terrestrial lead isotope evolution by a two-stage model. Earth Planet Sci Lett 26:207–221

Sun SS, McDonough WF (1989) Chemical and isotopic systematics of oceanic basalts: implications for mantle composition and processes. In: Saunders AD, Norry MJ (eds) Magmatism in ocean basins. Geol Soc Lond Spec Publ 42:313–345

Wang CY, Zhang Q, Qian Q, Zhou MF (2004) Geochemistry of the Early Palaeozoic Baiyin volcanic rocks (NW China): implications for the tectonic evolution of the North Qilian orogenic belt. J of Geol. 113:83–94

Wiedenbeck M, Alle P, Corfu F, Griffin WL, Meier M, Oberli F, Vonquadt A, Roddick JC, Speigel W (1995) 3 Natural Zircon standards for U-Th-Pb, Lu-Hf, trace-element and REE analyses. Geostand Newslett 19:1–23

Wood BJ, Virgo D (1989) Upper mantle oxidation state: ferric iron contents of lherzolite spinels by 57Fe Mössbauer spectroscopy and resultant oxygen fugacities. Geochim Cosmoch Acta 53:1277–1291

Wright JE, Shervais JW (Eds) (2008) Ophiolites, Batholiths, and regional geology: a session in Honor of Cliff Hopson. Geol Soc Am Spec Paper 438:1–572

Zappettini EO, Blasco G, Villar LM (1994) Geología del extremo sur del Salar de Pocitos, Provincia de Salta, República Argentina. VII Congr Geol Chil Actas I:220–224

Zimmermann U (1999) Sedimentpetrographische, geochemische und isotopengeochemische Methoden zur Bestimmung der Beziehung von Provenienz und Ablagerungsraum an aktiven Kontinentalrändern: Das ordovizische Back-Arc-Becken in der Süd-Puna, Hochland im Nordwesten Argentiniens. PhD-Thesis, University of Heidelberg, Germany

Zimmermann U (2005) Provenance studies of very low- to low-grade metasedimentary rocks of the Puncoviscana Formation in Northwest Argentina. In: Vaughan APM, Leat PT, Pankhurst RJ (eds) Terrane processes at the margins of Gondwana. Geol Soc Lond Spec Publ 246:381–416

Zimmermann U, Bahlburg H (2003) Provenance analysis and tectonic setting of the Ordovician deposits in the southern Puna basin, NW Argentina. Sedimentology 50:1079–1104

Zimmermann U, Bahlburg H (2005) The crustal evolution of the Central Andes during the Neoproterozoic to the Silurian. Geochim Cosmoch Acta 69-10S:A877

Zimmermann U, van Staden A (2002a) Neoproterozoic to pre-Ordovician very-low to low-grade metasedimentary rocks from Sijan (Sierra de Ambato) and Campo Volcán (Puna) in northwestern Argentina. XIV Congr Geol Argent Actas I:229–234

Zimmermann U, van Staden A (2002b) The stratigraphy of Lower Palaeozoic rocks from the southern Sierra de Calalaste (Northwest Argentina). 16th Int Sed Congr Actas II:421–422

Zimmermann U, Moya MC, Bahlburg H (1998) New evidence for the stratigraphic subdivision of Ordovician sedimentary successions in the Southern Puna (NW Argentina) based on graptolites. Terra Nostra 98:179–180

Zimmermann U, Luna Tula G, Marchioli A, Narváez G, Olima H, Ramírez A (2002) Análisis de la procedencia de la Formación Falda Ciénaga (Ordovícico Medio, Puna Argentina) por petrografía sedimentaria, elementos trazas e isotopía de Nd. Assoc Argent Sed Rev 9:1–24

Zimmermann U, Niemeyer H, Meffre S (2010) Revealing the continental margin of Gondwana: the Ordovician arc of the Cordón de Lila (northern Chile). Int J Earth Sci 99-S1:S39–S56